Journal of Power Sources 253 (2014) 366–372

Contents lists available at ScienceDirect

Journal of Power Sources

journal homepage: www.elsevier.com/locate/jpowsour

Nanosized Ge@CNF, Ge@C@CNF and Ge@CNF@C composites *via* chemical vapour deposition method for use in advanced lithium-ion batteries

Shuli Li [a], Chen Chen [a], Kun Fu [a], Ryan White [b], Chengxin Zhao [c], Philip D. Bradford [a], Xiangwu Zhang [a,*]

[a] Fiber and Polymer Science Program, Department of Textile Engineering, Chemistry and Science, North Carolina State University, Raleigh, NC 27695-8301, USA
[b] Department of Materials Science and Engineering, North Carolina State University, Raleigh, NC 27695-8301, USA
[c] Department of Physics, University of Oslo, Oslo 0316, Norway

HIGHLIGHTS

- Three distinct Ge-filled CNF composites fabricated by CVD and electrospinning.
- CNF matrix and CVD carbon layer enhance the structural integrity of Ge anode.
- Ge@CNF@C exhibits high capacity retention due to the thorn-like Ge morphology.

GRAPHICAL ABSTRACT

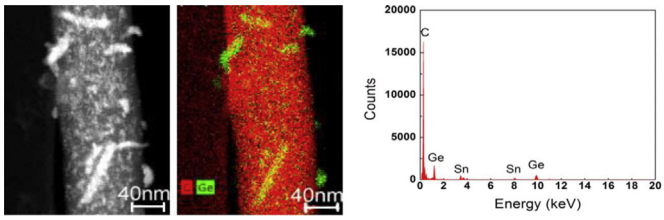

ARTICLE INFO

Article history:
Received 10 September 2013
Received in revised form
21 November 2013
Accepted 4 December 2013
Available online 21 December 2013

Keywords:
Lithium alloy
Germanium
Chemical vapor deposition
Electrospinning
Lithium-ion battery

ABSTRACT

Three distinct Ge nanoparticle-filled carbon nanofiber (CNF) composites, Ge@CNF, Ge@C@CNF and Ge@CNF@C, were fabricated by chemical vapor deposition (CVD) and electrospinning techniques. These different structures were prepared by: 1) dispersing Ge nanoparticles into CNF, 2) adding carbon-coated Ge nanoparticles (Ge@C) prepared by CVD into CNF, and 3) depositing CVD carbon onto Ge@CNF, respectively. Compared with the Ge@CNF composite, both Ge@C@CNF and Ge@CNF@C had additional amorphous carbon coating fabricated by the CVD method. The three composites were studied as binder-free electrodes for rechargeable lithium-ion batteries. Raw Ge anode materials suffered from serious volume changes and nanoparticle aggregations during cycling, resulting in pulverization and capacity loss. However, carbon nanofiber and the supplemental CVD carbon layer in these nanofiber composites could help preserve the structural integrity of the alloy anode materials during repeated cycling, and consequently, lead to improved cycling stability. In this work, it was found that among the three composites, Ge@CNF@C exhibited the highest capacity retention of 89% at the 50th cycle due to the structurally-durable thorn-like Ge morphology and the additional CVD carbon confinement. Ge@CNF and Ge@C@CNF encountered rapid capacity loss because large Ge clusters were formed and jeopardized the integrity of the electrode structure during cycling.

1. Introduction

Rechargeable lithium-ion batteries have long been considered as an attractive power source for portable electronics, electric vehicles, and emerging smart grids [1]. One major challenge in the design of high-performance lithium-ion batteries is to maintain the

* Corresponding author.
E-mail address: xiangwu_zhang@ncsu.edu (X. Zhang).

0378-7753/$ – see front matter © 2013 Elsevier B.V. All rights reserved.
http://dx.doi.org/10.1016/j.jpowsour.2013.12.017

structural stability of the electrodes during repeated lithium insertion and extraction [2–4]. For example, alloying anodes, such as Si, Ge, Sn, Pb, Al, Au and Mg, possess high lithium storage ability but suffer from large volume change during cycling. To address this issue, alloying anodes have been modified by downsizing the bulk materials to the nanoscale, dispersing the elements into carbon matrices, or preparing intermetallic alloying materials [5–7]. Recently, Li et al. fabricated a nano-Si anode material by laser-induced silane gas reaction and obtained a high reversible capacity of 1700 mAh g^{-1} after ten cycles [8]. Ji et al. reported the preparation of Si/C composite nanofibers by embedding Si nanoparticles in electrospun carbon nanofibers. The Si/C composite nanofibers exhibited a reversible capacity of around 800 mAh g^{-1} and a capacity retention of 85% after twenty cycles [3,4,9,10]. Moreover, Li et al. prepared a $FeSi_6$/graphite composite by a simple mechanical ball milling method. The composite anode offered a large reversible capacity of 800 mAh g^{-1} and improved cyclability due to the buffering effect of the inactive $FeSi_2$ phase and graphite layers on the volumetric change of the Si phase during alloying reaction [11].

Among the various alloying anodes, Si has been the focus of recent research, while Ge, another high-capacity material (theoretical capacity: 1600 mAh g^{-1}), has received less attention. Compared to Si, Ge has smaller volume change and higher lithium diffusion coefficient, and thus is a competitive anode material [12]. Cui et al. prepared Ge/carbon composite nanospheres and Ge/carbon nanotubes through a pyrolysis technique and obtained capacities of more than 900 and 700 mAh g^{-1}, respectively [13,14]. Recently, Woo et al. fabricated Ge nanowire/graphite nanofiber composites by chemical vapor deposition (CVD). These composites also showed large reversible capacities and high rate capability due to the extensive entanglement and large contact area between the Ge nanowires and graphite nanofibers [15]. Although promising electrode systems have recently been proposed, the cycling performance of most Ge-based anodes is still limited by the relatively large volumetric change of Ge particles, which cannot be accommodated completely by using only one carbon layer confinement.

In this work, we prepared new Ge@CNF, Ge@C@CNF and Ge@CNF@C structures by: 1) dispersing Ge nanoparticles into carbon nanofibers (CNF), 2) adding carbon-coated Ge nanoparticles (Ge@C) prepared by chemical vapor deposition (CVD) into CNF, and 3) depositing CVD carbon onto the surface of Ge@CNF, respectively. The schematic of the three structures and their fabrication processes are illustrated in Fig. 1. In Ge@C@CNF and Ge@CNF@C structures, two carbon confinement structures were formed on the Ge active material, including the amorphous carbon coating fabricated by the CVD method and the CNF matrix by electrospinning. The amorphous carbon coating deposited by CVD can accommodate the cracking of Ge nanoparticles in Ge@C@CNF and the pulverization of the integral Ge@CNF structure in Ge@CNF@C during lithiation and delithiation processes. In addition, the combination of electrospinning and carbonization methods leads to durable electron-conducting non-woven CNF webs that can be used as flexible binder-free electrodes. The absence of polymer binder

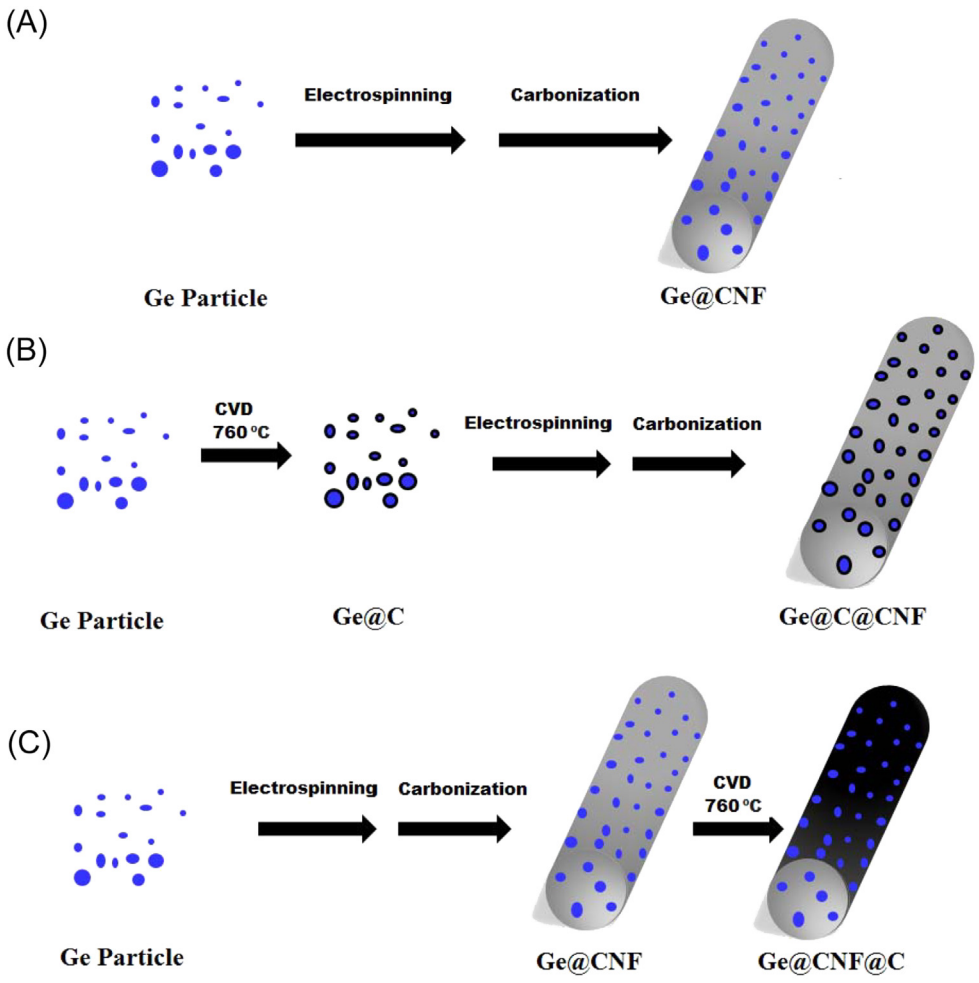

Fig. 1. Schematic illustrating the fabrication processes of (A) Ge@CNF, (B) Ge@C@CNF, and (C) Ge@CNF@C.

in our battery electrode system prevents the separation of active materials from the electrolyte, resulting in reduced electrode–electrolyte interface and enhanced electrode reaction kinetics. Therefore, by carefully designing nanoparticle-filled CNF composites with controlled structures, the electrochemical performance of Ge-based electrodes would be enhanced and thus the impact of changing variable structures is of great importance and needs further exploration. It must be noted that Ge is more expensive than other high-energy anode materials such as Si and Sn. However, since Ge is able to provide more stable cycling performance than Si and higher discharge capacity than Sn, carefully-designed Ge-based CNF composite anodes can be used in high-energy lithium-ion batteries for electronic devices such as laptops and cell phones although they have to face a cost barrier in the electric vehicle application.

2. Experimental

Ge nanoparticles (70–100 nm) were purchased from SkySpring Nanomaterials. Polyacrylonitrile (PAN, Mw = 150,000) and solvent *N*,*N*-dimethylformamide (DMF) were supplied by Sigma Aldrich. All materials were used without further purification.

The preparation procedures of Ge@CNF, Ge@C@CNF, and Ge@CNF@C are shown in Fig. 1. For the preparation of Ge@CNF (Fig. 1A), Ge nanoparticles (30 wt% compared to PAN) were added directly into a DMF solution of PAN (8 wt%) at 60 °C. Mechanical stirring was applied for at least 24 h in order to ensure that the dispersion was homogeneous. To obtain composite nanofibers, a high-voltage power supply (Gamma ES40P-20W/DAM) was used to provide a voltage at around 15 kV during the electrospinning. Dry fibers were accumulated on the collector and formed fibrous mats. The electrospun Ge@PAN nanofibers were first stabilized in an air environment at 280 °C for 5.3 h (heating rate: 5 °C min^{-1}), and then carbonized at 700 °C for 1 h in an argon atmosphere (heating rate: 2 °C min^{-1}) to form Ge@CNF.

For Ge@C@CNF (Fig. 1B), Ge nanoparticles were first coated by CVD amorphous carbon using an ASM 6″ LPCVD with operating temperature and pressure of 760 °C and 10 Torr, respectively. Pure C_2H_2 gas was used as the carbon precursor with a flow rate of 200 sccm. The deposition time used was 60 min. The resultant Ge@C nanoparticles (30 wt% compared to PAN) were dispersed into a DMF solution of PAN (8 wt%) to obtain Ge@C@PAN electrospun nanofibers. The final product Ge@C@CNF was obtained after stabilizing and carbonizing Ge@C@PAN under the same conditions as used for Ge@CNF.

For Ge@CNF@C (Fig. 1C), 30 wt% Ge nanoparticles (compared to PAN) were first added into a DMF solution of 8 wt% PAN, which was then electrospun into Ge@PAN nanofibers. The electrospun Ge@PAN nanofibers were carbonized to form Ge@CNF. The final product Ge@CNF@C was obtained by depositing CVD carbon on Ge@CNF. The electrospinning, carbonization and CVD processing conditions used for Ge@CNF@C were the same as those for Ge@C@CNF.

The morphology of the resultant Ge@CNF, Ge@C@CNF, and Ge@CNF@C was observed with scanning electron microscope (SEM) (JEOL 6400F Field Emission SEM at 5 kV) and transmission electron microscopy (Hitachi HF-2000 TEM at 200 kV). Elemental Analyzer (Perkin Elmer, CHN 2400) was used to determine the composition of composites. The Ge contents of Ge@CNF, Ge@C@CNF and Ge@CNF@C composites were 54.5%, 55.7%, and 56.2 wt%, respectively.

Electrochemical experiments were carried out using coin-type half cells containing Ge@CNF, Ge@C@CNF and Ge@CNF@C as the working electrodes and Li foil as the counter electrode. The as-prepared Ge@CNF, Ge@C@CNF and Ge@CNF@C formed free-standing electronically-conductive fiber mats, and they were attached onto copper foil (Lyon industries, 0.025 mm thick) to be used as the working electrodes. The loadings of the working electrodes were 0.49, 0.40, and 0.43 mg cm^{-2} for Ge@CNF, Ge@C@CNF, and Ge@CNF@C, respectively. The separator used was Celgard® 2400 (Celgard LLC). The electrolyte was a 1 M $LiPF_6$ solution in ethylene carbonate (EC)/dimethyl carbonate (DMC) (1:1 v/v). The electrochemical performance was evaluated by carrying out galvanostatic charge–discharge experiments at 50 mA g^{-1} (C/32) between 0.01 and 2.00 V. The capacities were calculated based on the total weights of both Ge and carbon materials in the electrodes.

Reproducibility was assessed by preparing and testing all composites for three times.

3. Results and discussion

3.1. Morphology

The SEM images of Ge@CNF, Ge@C@CNF, and Ge@CNF@C are represented in Fig. 2. Large particle clusters can be observed in Ge@CNF (Fig. 2A) and Ge@C@CNF (Fig. 2B), indicating non-uniform dispersion of Ge and Ge@C nanoparticles in the CNF matrix. Compared with Ge@CNF, the Ge@C@CNF composite contains an extra CVD carbon coating layer on Ge particles, which increases the loaded nanoparticle size and leads to larger particle aggregations. However, as shown in Fig. 2C, there are fewer Ge clusters in Ge@CNF@C, suggesting an improved dispersion of Ge particles in these nanofibers.

From Fig. 2, it is also seen that Ge@CNF@C has smaller fiber diameters than Ge@C@CNF and Ge@CNF. The smaller diameter of Ge@CNF@C is probably caused by high-temperature CVD treatment applied to the fibers. When preparing Ge@CNF@C, Ge particles were first dispersed in the CNF matrix and the subsequent CVD coating process at 760 °C reduced the fiber diameter by further thermal deformation and removal of residual non-carbon elements from the fiber matrix. These SEM results indicate that the dispersion of nanoparticles with varying sizes and the processing order of CVD treatment have great influence on the surface morphology of the resultant fibers.

Detailed nanostructures of Ge@CNF, Ge@C@CNF and Ge@CNF@C were investigated with TEM technique and the results are illustrated in Fig. 3. The composite nanofibers were grounded and ultrasonically treated prior to TEM observation. As shown in Fig. 3A and B, large Ge nanoparticle clusters were formed and dispersed in the carbon matrix, especially in Fig. 3B, where a void of around 700 nm × 200 nm was formed due to the falling off of a Ge cluster during TEM sample preparation. This figure is a representative image of Ge@C@CNF and such defect (*i.e.*, void) can be commonly seen in Ge@CNF@C samples. The void indicates serious aggregation of Ge@C nanoparticles in the fiber matrix, which may exacerbate the pulverization of the particles and lead to rapid capacity loss during cycling when this material is used as a lithium-ion battery anode. However, from Fig. 3C, it is seen that Ge@CNF@C shows homogenously distributed Ge thorns of 50–100 nm embedded in or attached on the surface of the CNF matrix.

To further investigate the unique structure of Ge@CNF@C, high-resolution TEM image, atomic resolution elemental mapping and energy-dispersive X-ray spectroscopy (EDX) spectrum were obtained (Fig. 4). The TEM image shows a Ge@CNF@C nanofiber with thorn-like structures of around 10 nm in width and 30–80 nm in length (Fig. 4A). The composition of the nanofiber and the thorn-like structure were investigated by elemental mapping technique. The nanofiber and the thorn-like structures are composed of carbon and Ge, respectively, as indicated by elemental mapping (Fig. 4B). The EDX spectrum presents two characteristic peaks at 1 and 10 keV, which are typical for Ge element, as well as a 0.5 keV peak for carbon (Fig. 4C). Sn impurities are also detected in the spectrum. These results indicate that the thorn-structures are formed by Ge during the CVD treatment at 760 °C. It is likely that

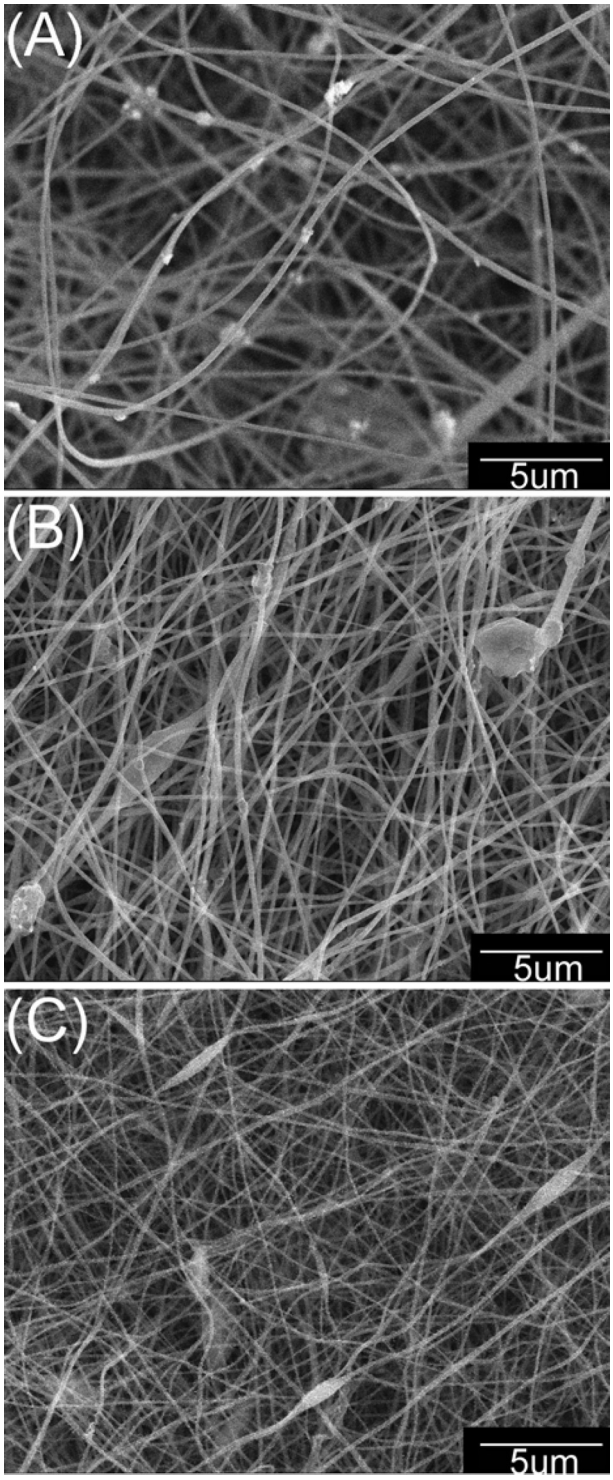

Fig. 2. SEM images of (A) Ge@CNF, (B) Ge@C@CNF, and (C) Ge@CNF@C.

the formation of Ge thorns is facilitated by the Sn impurities, which function as catalyst particles for the regrowth of Ge during CVD treatment. There are recent reports on the formation of Ge thorns facilitated by metal catalysts, such as Sn, Au, Ni, Cu, Co. For example, Er-doped SnO_2 nanofibers were used to obtain similar Ge thorns or nanorods through CVD method by Wu et al [16]. In that work, it was assumed that the system involved with the reduction of the trace amount of Sn and corresponding oxidation of Ge, followed by a thermal equilibrium between Sn and Ge, and the excess Ge resulted

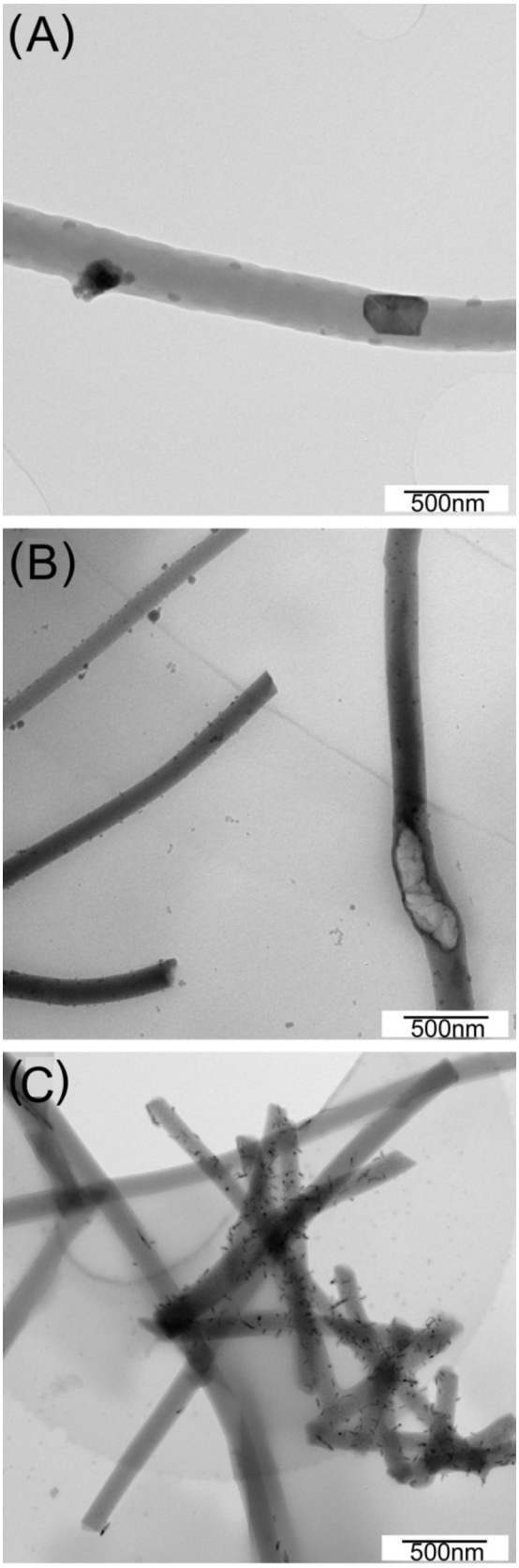

Fig. 3. TEM images of (A) Ge@CNF, (B) Ge@C@CNF, and (C) Ge@CNF@C.

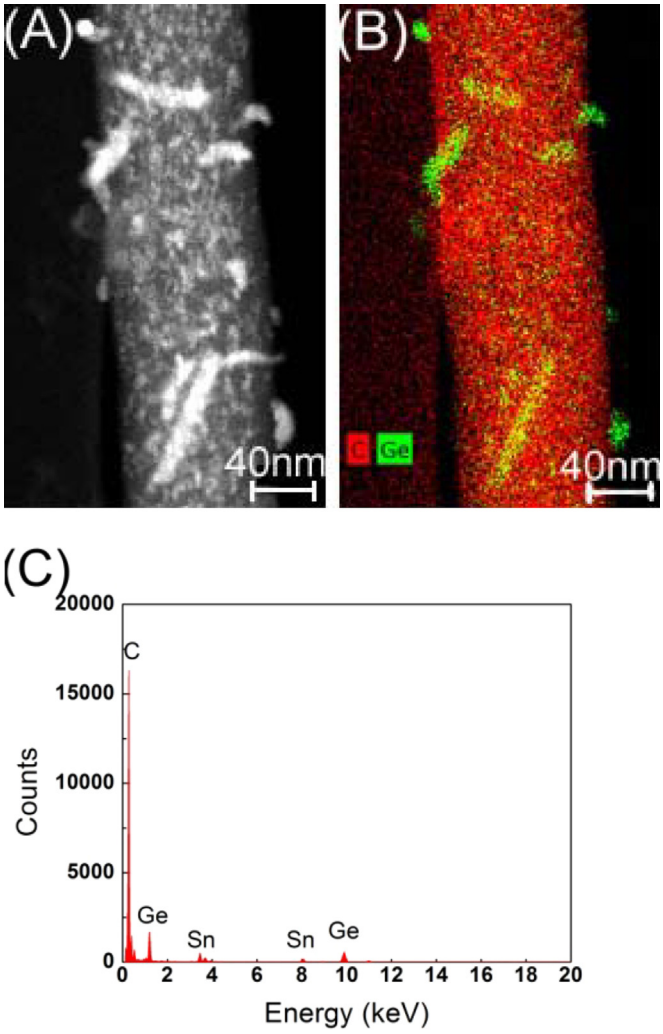

Fig. 4. (A) High-resolution STEM image, (B) atomic resolution elemental map, and (C) EDX spectrum of Ge@CNF@C. In the atomic resolution elemental map, Ge and carbon elements are colored with light green and red, respectively. (For interpretation of the references to color in this figure legend, the reader is referred to the web version of this article.)

in vapor–liquid–solid-type growth of Ge nanorods. In the alloy form, Sn and Ge were able to form an eutectic system with a critical temperature of 231 °C. Above the critical temperature, the growth of Ge thorns could be initiated with the help of Sn catalyst. Recently, Meng's group investigated the effects of different catalytic metals (Au, Ni, Cu, Co) on the yield and quality of Ge thorns during the CVD process [17]. They discussed the essentiality of the catalytic metals for providing catalytic nucleation sites for the growth of Ge thorns inside the channels of the anodic aluminum oxide template. Once the Ge nanocrystal seeds on the catalyst surface were formed, the subsequent growth of Ge thorns would continue by itself, which would be highly dependent on the type of the catalyst. Similarly, in our work, the Sn impurities presumably served as a catalyst that facilitated the formation of Ge thorns during CVD treatment.

To further understand the structure of Ge@CNF, Ge@C@CNF, and Ge@CNF@C, their Raman spectra were obtained and are shown in Fig. 5. For comparison, the Raman spectrum of Ge@C particles is also shown. For all four samples, a strong D-band at around 1350 cm^{-1} and a relatively small G-band at 1600 cm^{-1} are observed. The D-band can be explained as defect- and disorder-induced features in the graphene layers of carbon materials, while the G-band is indicative of the high-frequency E_{2g} first-order

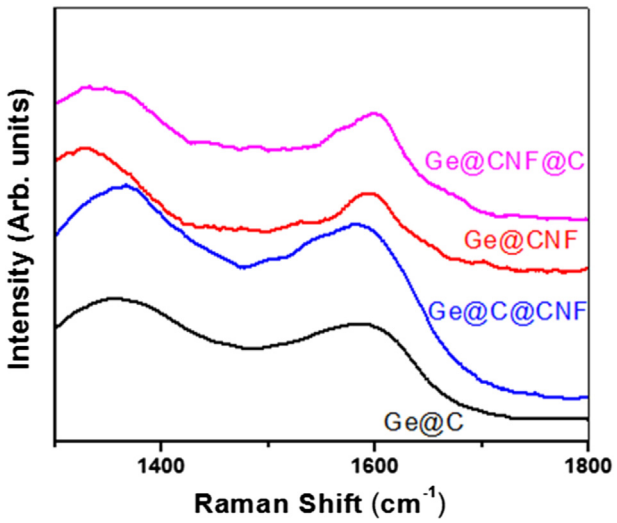

Fig. 5. Raman spectra of Ge@C, Ge@CNF, Ge@C@CNF, and Ge@CNF@C.

graphitic crystallites of the carbon. The presence of the strong D band suggests that the carbon component has a typical disordered graphitic structure with low crystallinity and graphitization [18]. The intensity ratio of D peak to G peak, denoted by $R_I = I_D/I_G$, is a good indication of the carbon structure, and a higher R_I value typically reveals a more disordered carbon structure. As shown in Fig. 5, the R_I values of Ge@C, Ge@CNF, Ge@C@CNF, and Ge@CNF@C are 1.358, 1.074, 1.106 and 1.103, respectively. Ge@C has a higher R_I value than Ge@CNF, suggesting that the carbon coating created by CVD is more amorphous or disordered than the CNF matrix.

3.2. Electrochemical performance

Three as-prepared nanofiber composites, *i.e.*, Ge@CNF, Ge@C@CNF and Ge@CNF@C, were collected in the form of free-standing nanofiber mats and they were directly used as the working electrodes in lithium-ion half cells without any polymer binders or carbon black conductor. Herein, we investigated both Galvanostatic charge–discharge phenomena and differential capacity curves of Ge@CNF, Ge@C@CNF and Ge@CNF@C nanofiber composite anodes.

Galvanostatic charge–discharge experiments were carried out at a current density of 50 mA g^{-1} within a voltage window of 0.01–2.00 V to evaluate the electrochemical performance. Fig. 6 displays galvanostatic charge–discharge curves of the first, second and twentieth cycles of Ge@CNF, Ge@C@CNF and Ge@CNF@C. In the first cycle, the voltage of all three composites drops rapidly during the discharge process from 2.00 V to about 0.7, 0.4 and 1.2 V, respectively, followed by a small plateau and a sloping line smoothly downshifting to 0.01 V. This small plateau is known as the result of the decomposition of electrolyte solution and the formation of the solid electrolyte interface (SEI), which covers the electrode surface and hinders the electrolyte from further decomposition [10,19]. From Fig. 6, it is also seen that Ge@CNF and Ge@CNF@C exhibit smaller initial capacity losses than Ge@C@CNF. In the first cycle, Ge@CNF, Ge@C@CNF and Ge@CNF@C show specific discharge capacities of 1385, 1070, and 1466 mAh g^{-1}, and charge capacities of 808, 252, and 626 mAh g^{-1}, respectively. The irreversible capacities of 577, 818, and 840 mAh g^{-1} can be mainly ascribed to the formation of the SEI film during the first cycle. The Ge@C@CNF composite has the lowest charge capacity, which is the consequence of the large volume expansion of aggregated Ge@C

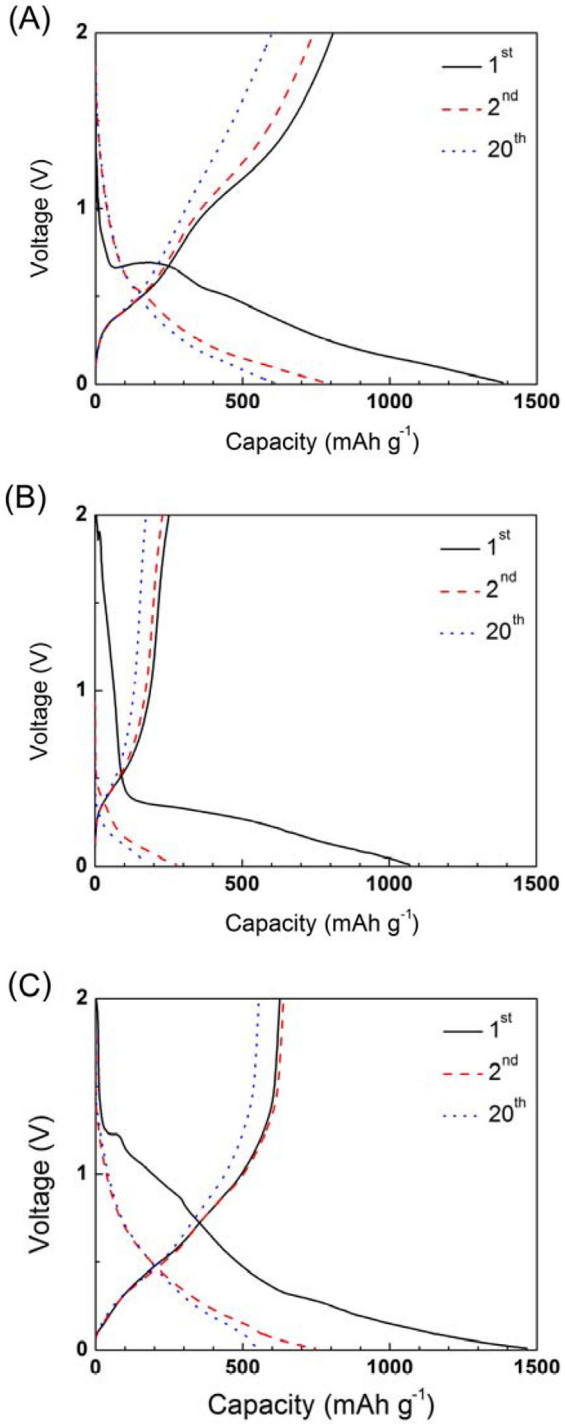

Fig. 6. Galvanostatic charge–discharge curves of the first, second and twentieth cycles of (A) Ge@CNF, (B) Ge@C@CNF, and (C) Ge@CNF@C.

nanoparticles during the formation of Li_xGe and subsequent detachment of the nanoparticles from the CNF matrix. This agrees with the TEM result shown in Fig. 3B.

From Fig. 6, it is also seen that at the second cycle, the voltage plateau disappears, indicating a stable SEI has formed. As a result, all three composites exhibit coulombic efficiencies of over 95% at the second cycle. At the same time, the discharge capacities of Ge@CNF, Ge@C@CNF, and Ge@CNF@C are around 781, 278, and 747 mAh g^{-1}, and their charge capacities are around 741, 229, and 639 mAh g^{-1}, respectively. Similar to the first cycle, the Ge@C@CNF composite has the lowest Li storage ability due to the detachment of the particle clusters. Among all three composites, the relatively homogenous dispersion of Ge and good confinement of carbon material in Ge@CNF@C (Fig. 3C) result in the most stable cyclability for this anode material. At the twentieth cycle, both charge and discharge capacities reduce slightly. The coulombic efficiencies of all three composites are still greater than 95%.

Differential capacity curves of the first and second cycles of Ge@CNF, Ge@C@CNF, and Ge@CNF@C are plotted in Fig. 7. In the lithium alloying process, peaks indicate the lithium insertion into equipotential sites, and the presence of multiple sharp peaks at the first cycle suggests the formation of a number of different Li_xGe_y phases during electrochemical lithiation [20]. In Fig. 7, the voltage values (0.50–1.10, 0.30–0.50, 0.15–0.30, and 0–0.15 V) are consistent with those reported for Li_9Ge_4, Li_7Ge_2, $Li_{15}Ge_4$, and $Li_{22}Ge_5$ during lithium insertion [12,20–22]. However, the peaks at 0.69 V (Fig. 7A) and 0.35 V (Fig. 7B) during lithium alloying process are mainly ascribed to the SEI formation, which confirms the results shown in Fig. 6. The peak at 1.26 V in Fig. 7C is attributed to the irreversible lithium-ion insertion process in the disordered carbon [23,24]. From Fig. 7, it is also seen that typical dealloying reactions of Ge occur at around 0.4 and 1.0 V for Ge@C and Ge@CNF@C. The differential capacity plots of Ge@CNF and Ge@CNF@C in the second cycle also confirm that Ge actively involves in the alloying and dealloying processes due to the presence of broad peaks, which also suggest that Ge has turned into amorphous in this cycle. On the other hand, during the delithiation process of the Ge@C@CNF, only the peak at 0.4 V appears and this is mainly attributed to the dealloying of carbon (Fig. 7B). The lack of the peak at 1.0 V suggests the serious detachment of the Ge@C clusters from the CNF matrix.

The cycling performance of Ge@CNF, Ge@C@CNF, and Ge@CNF@C is presented in Fig. 8. For comparison, the cycling performance of pure carbon nanofibers is also shown. Compared with pure carbon nanofibers, Ge@CNF@C and Ge@C@CNF achieved better discharge capacity and cycling performance. It is also observed that during cycling, Ge@CNF@C exhibits more stable capacities than Ge@CNF and Ge@C@CNF. The significant capacity loss of Ge@C@CNF is mainly caused by the severe volume change of large Ge clusters during lithium insertion and extraction. The enormous agglomeration and volume change of the Ge clusters lead to severe particle separation and pulverization of the anode structure. On the other hand, Ge@CNF@C has the most stable structure and can better tolerate the volume change upon repeated lithium insertion and extraction, and hence it exhibits the best cycling performance. As shown in Fig. 8, Ge@CNF@C exhibits the highest capacity retention of 89% with a relatively large reversible capacity of 553 mAh g^{-1} at 50th cycle. In Ge@CNF@C, the thorn-like Ge structure possesses high aspect ratio, which is more structurally durable during Li insertion and extraction. Moreover, the CVD carbon coating on the outer surface of Ge@CNF further constrains the volume change of the Ge nanoparticles and consequently contributes to the good stability of the electrode structure. As a result, among the electrode materials studied, Ge@CNF@C is the most promising anode material for high-energy lithium-ion batteries.

4. Conclusion

Ge@CNF, Ge@C@CNF and Ge@CNF@C were prepared by using two different carbon materials, amorphous carbon coating by CVD and carbon nanofiber matrix by electrospinning technique, to mitigate the large volume change of Ge nanoparticles and preserve the integrity of the anode structure during cycling. These binder-free electrode materials showed dissimilar characteristics in terms of structural morphology and electrochemical performance,

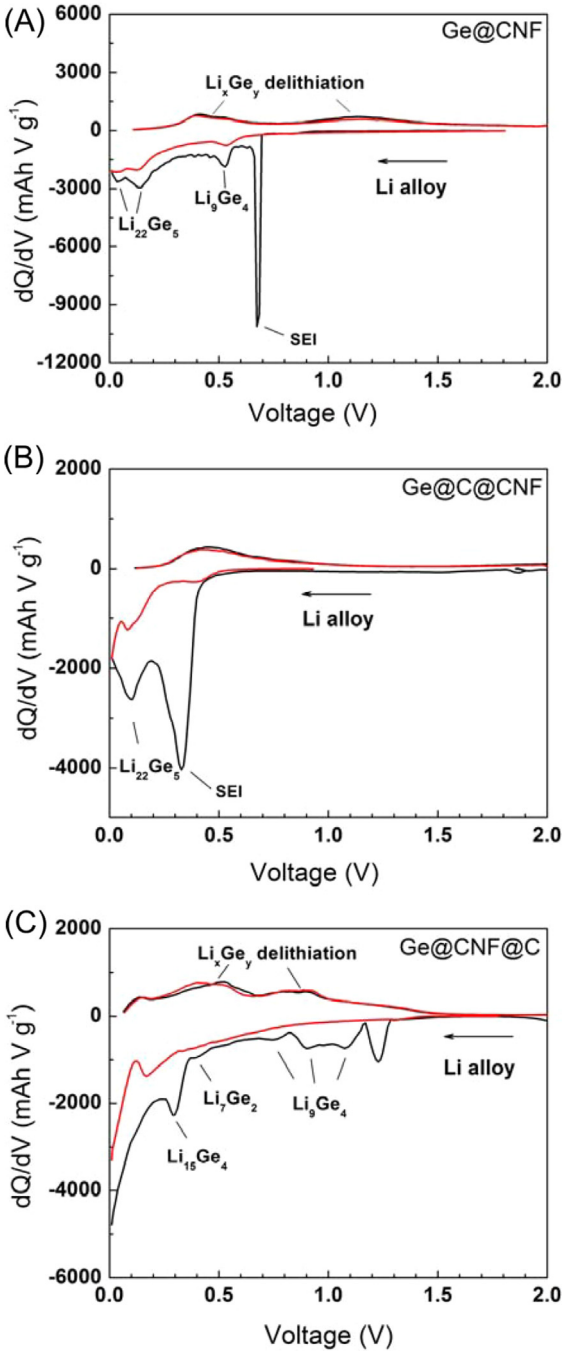

Fig. 7. Differential capacity plots of the first and second cycles of (A) Ge@CNF, (B) Ge@C@CNF, and (C) Ge@CNF@C.

which were demonstrated by SEM, TEM, Raman spectroscopy, and galvanostatic charge–discharge results. Ge@C@CNF showed significant capacity loss during cycling due to enormous agglomeration and volume change of Ge particles and the subsequent pulverization of the anode structure. On the other hand, Ge@CNF@C exhibited the highest capacity retention of 89% and the largest reversible capacity of 550 mAh g^{-1} at 50th cycle because of two carbon confinement structures and the unique Ge thorn morphology. In Ge@CNF@C, the CVD carbon coating and CNF matrix effectively constrained the volume change of Ge material and consequently maintained the electrode integrity. In addition, the Ge thorns in Ge@CNF@C possessed high aspect ratio, possibly

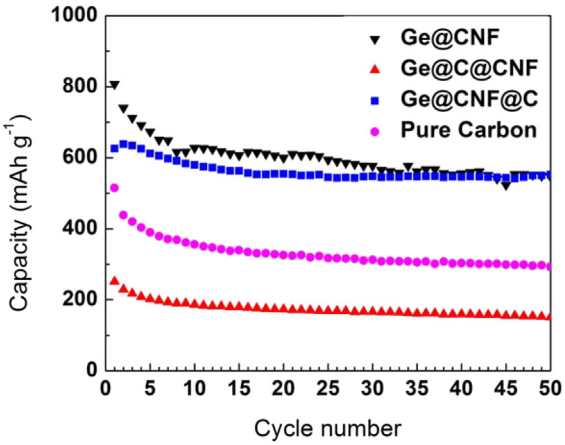

Fig. 8. Cycling performance of Ge@CNF, Ge@C@CNF, and Ge@CNF@C. For comparison, the cycling performance of pure carbon nanofibers is also shown.

notable mechanical stability and short lithium diffusion length, which facilitated the relatively high reversible capacities and excellent cycling performance.

Acknowledgments

This research was supported by the U.S. Department of Energy under Grant No: DE-EE0001177, Advanced Transportation Energy Center, and ERC Program of the National Science Foundation under Award Number EEC-08212121.

References

[1] P. Poizot, S. Laruelle, S. Grugeon, L. Dupont, J.M. Tarascon, Nature 407 (6803) (2000) 496–499.
[2] H. Lee, H. Kim, S.G. Doo, J. Cho, J. Electrochem. Soc. 154 (4) (2007) A343–A346.
[3] L.W. Ji, X.W. Zhang, Energy Environ. Sci. 3 (1) (2010) 124–129.
[4] L.W. Ji, X.W. Zhang, Electrochem. Commun. 11 (6) (2009) 1146–1149.
[5] M. Holzapfel, H. Buqa, W. Scheifele, P. Novak, F.M. Petrat, Chem. Commun. 12 (2005) 1566–1568.
[6] C.M. Park, J.H. Kim, H. Kim, H.J. Sohn, Chem. Soc. Rev. 39 (8) (2010) 3115–3141.
[7] W.J. Zhang, J. Power Sources 196 (1) (2011) 13–24.
[8] H. Li, X.J. Huang, L.Q. Chen, Z.G. Wu, Y. Liang, Electrochem. Solid State 2 (11) (1999) 547–549.
[9] L.W. Ji, Z. Lin, M. Alcoutlabi, X.W. Zhang, Energy Environ. Sci. 4 (8) (2011) 2682–2699.
[10] L.W. Ji, K.H. Jung, A.J. Medford, X.W. Zhang, J. Mater. Chem. 19 (28) (2009) 4992–4997.
[11] T. Li, Y.L. Cao, X.P. Ai, H.X. Yang, J. Power Sources 184 (2) (2008) 473–476.
[12] J. Graetz, C.C. Ahn, R. Yazami, B. Fultz, J. Electrochem. Soc. 151 (5) (2004) A698–A702.
[13] G.L. Cui, L. Gu, L.J. Zhi, N. Kaskhedikar, P.A. van Aken, K. Mullen, J. Maier, Adv. Mater. 20 (16) (2008) 3079–3083.
[14] G.L. Cui, L. Gu, N. Kaskhedikar, P.A. van Aken, J. Maier, Electrochim. Acta 55 (3) (2010) 985–988.
[15] S.H. Woo, S.J. Choi, J.H. Park, W.S. Yoon, S.W. Hwang, D. Whang, J. Electrochem. Soc. 160 (1) (2013) A112–A116.
[16] J. Wu, J.L. Coffer, Y.J. Wang, R. Schulze, J Phys. Chem. C 113 (1) (2009) 12–16.
[17] X.D. Li, G.W. Meng, Q.L. Xu, M.G. Kong, X.G. Zhu, Z.Q. Chu, A.P. Li, Nano Lett. 11 (4) (2011) 1704–1709.
[18] L.W. Ji, X.W. Zhang, Carbon 47 (14) (2009) 3219–3226.
[19] Y.S. Hu, R. Demir-Cakan, M.M. Titirici, J.O. Muller, R. Schlogl, M. Antonietti, J. Maier, Angew. Chem. Int. Ed. 47 (9) (2008) 1645–1649.
[20] S. Yoon, C.M. Park, H.J. Sohn, Electrochem. Solid State 11 (4) (2008) A42–A45.
[21] B. Laforge, L. Levan-Jodin, R. Salot, A. Billard, J. Electrochem. Soc. 155 (2) (2008) A181–A188.
[22] A.M. Chockla, M.G. Panthani, V.C. Holmberg, C.M. Hessel, D.K. Reid, T.D. Bogart, J.T. Harris, C.B. Mullins, B.A. Korgel, J. Phys. Chem. C 116 (22) (2012) 11917–11923.
[23] L. Wang, C.X. Ding, L.C. Zhang, H.W. Xu, D.W. Zhang, T. Cheng, C.H. Chen, J. Power Sources 195 (15) (2010) 5052–5056.
[24] K. Fu, L. Xue, O. Yildiz, S. Li, H. Lee, Y. Li, G. Xu, L. Zhou, P.D. Bradford, X. Zhang, Nano Energy 2 (5) (2013) 976–986.